A mechanistic model for the time-dependent autogenous shrinkage of high performance cementitious materials

Le Huang, Zhijian Chen, Hailong Ye*

Department of Civil Engineering, The University of Hong Kong, Hong Kong, China

* Corresponding author. E-mail: hlye@hku.hk

Abstract: An accurate prediction of time-dependent autogenous shrinkage behaviors of concrete, especially for high performance concrete (HPC) at an early age, is of great significance to assess and control the cracking risks of restrained structural elements. In this study, based on the capillary tension theory, a mechanistic model for evaluating the time-dependent autogenous shrinkage behaviors of high performance concrete is proposed. A total of 416 data points including the concrete composition, curing condition, age of concrete, water-to-cement (binder) ratio, internal relative humidity, elastic modulus, and measured autogenous shrinkage are selectively collected for the model establishment. The effects of silica fume on the development of autogenous shrinkage are also considered. Upon the sound physical basis, the model requires only a few parameter inputs related to the mixture proportion and physicochemical properties of components. The reasonable agreements between the analytical predictions and independent experimental results, as well as common used formulas from different codes (i.e., ACI 209, Eurocode 2, and Model Code 2010), demonstrate that the time-dependent evolution of autogenous shrinkage of HPC can be reasonably predicted by the model proposed in this study.

Keywords: time-dependent model; autogenous shrinkage; high performance concrete; capillary tension; silica fume

Nomenclature

ε_c	autogenous shrinkage	P_c	capillary tension
σ	surface tension of pore water	θ	contact angle between water and gel solid
r_c	radius of menisci	ρ, M	density and molar mass of the pore fluid
R	universal gas constant, 8.314 [J/(mol·K)]	T	Fahrenheit temperature
K_b	bulk moduli of the whole porous body	K_s	moduli of the solid skeleton
S_w	degree of saturation	RH	internal relative humidity
α	degree of hydration	w/c, w/b	water to cement (binder) ratio
t	age of concrete	T_{cri}	critical time related to RH
a_t, b_t	parameters related to the age of concrete	α, β, γ	parameters related to T_{cri}
V_{cw}, V_{gw}	volume of capillary water and gel water	V_{cs},	chemical shrinkage
E	elastic modulus	υ	Poisson's ratio
E_{28}	28 d elastic modulus	A	a constant related to E_{28}
p	initial porosity	s, c	weight of silica fume and cement
SF	mass percentage of silica fume, $s/(s+c)$	f_{ck}, f_{cm}	characteristic and mean compressive strengths of concrete at the age of 28 d

1. Introduction

After decades of rapid development, high performance concrete (HPC) has become one of the most recent types of construction materials applied routinely in critical civil infrastructure. Compared with normal performance concrete (NPC), HPC is generally characterized by using high-strength Portland cement, fine-grained sand, silica fume, and in many cases, an elimination of coarse aggregate [1,2]. Substantial research has demonstrated that upon such an innovative mixture, superior mechanical performance [3], better rheological properties [4] and durable resistance against environmental attacks [5] can be satisfactorily obtained. However, due to the high binder content and low water-to-binder ratio (< 0.4, in general), plus the pozzolanic effect of silica fume, the competition inside HPC between the developments of tensile strength and stress that evolves with hydration process is likely to be inclined to against the former [6]. Hence, the potential risk of autogenous shrinkage cracking of HPC induced by self-desiccation will be greatly amplified, as illustrated in Fig. 1. Although direct relation between this detrimental effect and structural premature failure has not been evidenced, it will significantly decrease the strength and durability of structures, particularly for those in harsh environments [7].

On the other hand, in some landmark projects or lifeline engineering, massive HPC is widely used and the volume of hardened blocks is quite remarkable [8]. In such cases, the majority of the non-load induced deformations of inner concrete, which may probably last for many decades, are related to the autogenous shrinkage, because other types of shrinkage are generally excluded [9]. Hence, under these circumstances, the development of autogenous shrinkage against time becomes one of the main issues that concern.

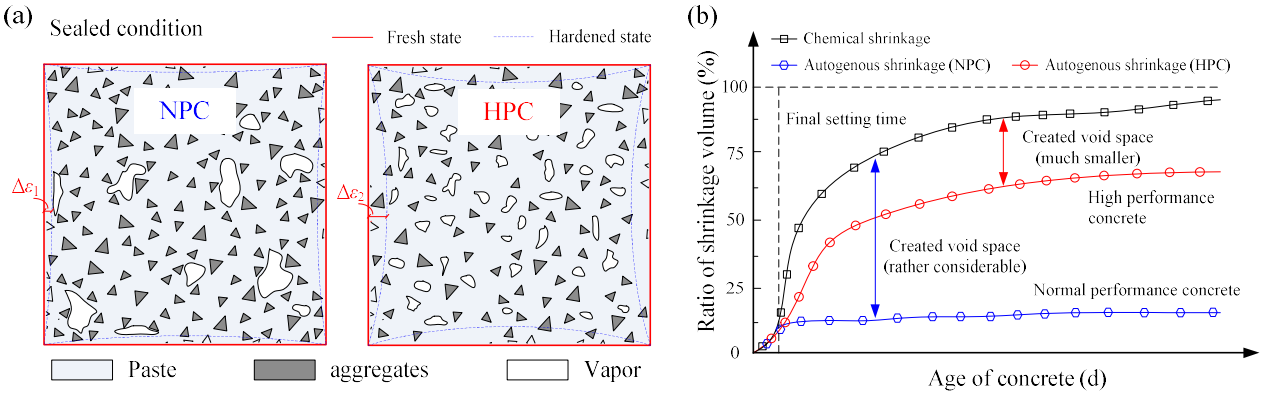

Fig. 1 Illustrative comparison of the autogenous shrinkage developed in NPC and HPC.

On account of these reasons, the autogenous shrinkage of HPC has been frequently reported in recent years [10,11]. Although the experimental results vary greatly due to the increasing diversification of material compositions, it has been commonly acknowledged to be one of the crucial causes of the immature cracking of young hardening concrete [12-14]. Regarding the formation mechanism of autogenous shrinkage, a general consensus also has been reached that the induced pressure differential in pores as the hydration process advances, termed capillary tension, is the main driving force, accompanied by the gradual reduction of internal relative humidity [15,16]. Hence, compared to conventional concrete, higher negative pore pressure is generated during self-desiccation as a consequence of lower w/b ratio and finer pore structure formed in HPC, resulting in a much larger autogenous shrinkage [17].

Concerning the quantitative evaluation of the development of autogenous shrinkage, the available analytical solutions can be roughly classified into three categories, i.e., pure mathematical models, empirical equations, and theoretical approaches [18-20]. The pure mathematical models may be most straightforward but of no physical significance [21]. For example, Nehdi et al. [22] built an artificial neural network model upon the artificial intelligence technique, which does not require any physical relationships between different variables. The empirical

equations generally use simple formulas incorporating the key variables by means of statistical analysis on numerous experimental results, which are widely adopted by standards or specifications from different countries [23-26]. For theoretically based approaches, the main probable governing mechanisms responsible for the shrinkage, like capillary tension [20], disjoining pressure [27], and surface free energy [28], all have been exploited so far. However, it should be noted that in general, the abovementioned models are limited to normal concrete with a compressive strength ranging from 30 to 60 MPa [29], and the effects of high contents (≥ 10%) of supplementary cementitious materials, especially the silica fume, are not taken into account [30].

Thus, the main purpose of this study is to propose a model for the evaluation of time-dependent autogenous shrinkage of HPC, based on the well-established capillary tension theory. To this end, hundreds of data points in terms of the composition of concrete, curing condition, age of concrete, water-to-cement (binder) ratio, internal relative humidity, elastic modulus, and measured autogenous shrinkage are selectively collected for the model establishment. It is hoped that upon the solid theoretical basis, followed by reliable independent validations, the proposed mechanistic-based model is of beneficial to better understand the autogenous shrinkage development in HPC, and estimate the potential cracking risk in the design of durable concrete infrastructure.

2. Overview of the capillary tension approach

Regarding the modelling of autogenous shrinkage of cementitious materials, the widely adopted capillary tension theory is regarded as the most appropriate approach for its sound mechanical and thermodynamic background [31]. In this section, a brief overview of the capillary tension theory is first presented.

2.1 Theoretical basis of capillary tension

For cementitious materials, it is generally thought that there is no evaporation occurs initially, because from a thermodynamic viewpoint, at this stage a vapor-water equilibrium is reached where the rate of evaporation is equal to that of condensation on a molecular level [32], as shown in Fig. 2 (a). However, as the hydration process advances, relative humidity *RH* gradually reduces from 100%, and the original vapor-water equilibrium is violated, resulting in the formation of menisci in the pores to restore the pressure balance, as shown in Fig. 2 (b).

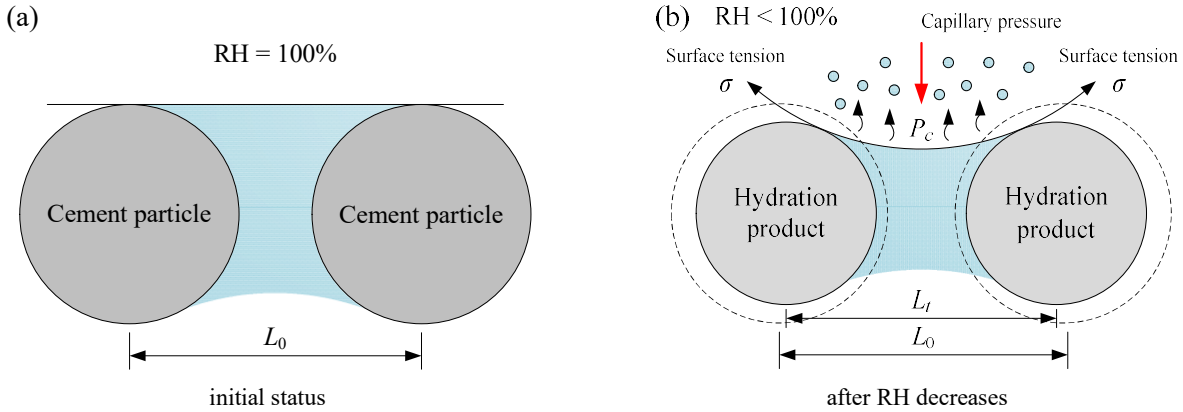

Fig. 2 Schematic illustration of the evolution of capillary tension during the hydration process.

Based on the Laplace equation [33], the difference between vapor pressure P_v and water pressure P_w, named capillary tension P_c, can be calculated as

$$P_c = P_v - P_w = -\frac{2\sigma\cos\theta}{r_c} \tag{1}$$

where σ is the surface tension of pore water, θ is the contact angle between water and gel solid, r_c is the radius of

menisci. With relative humidity *RH* further decreases, the curvature radius of menisci gradually reduces while its surface tension rises simultaneously, leading to a more pronounced pressure differential. This physical evolution can be characterized by the Kelvin equation as follows [34],

$$P_c = -\frac{\rho RT \ln\left(RH/100\right)}{M} \tag{2}$$

where ρ is the density of the pore fluid and M is its molar mass correspondingly, R = 8.314 [J/(mol·K)] is the universal gas constant, and T is the Fahrenheit temperature. In general, ρ = 1000 kg/m^3 and M = 18 ×10^{-3} kg/mol are roughly assumed.

2.2 Calculation of autogenous shrinkage

The Kelvin-Laplace equation shown in Eqs. (1) and (2) indicates that the radius of menisci is mainly dependent on the relative humidity *RH* and related water properties, regardless of the pore size, Hence, as illustrated in Fig. 3, for a given *RH*, the meniscus in all the pores are equal under otherwise identical conditions, generating a constant capillary tension among these pores.

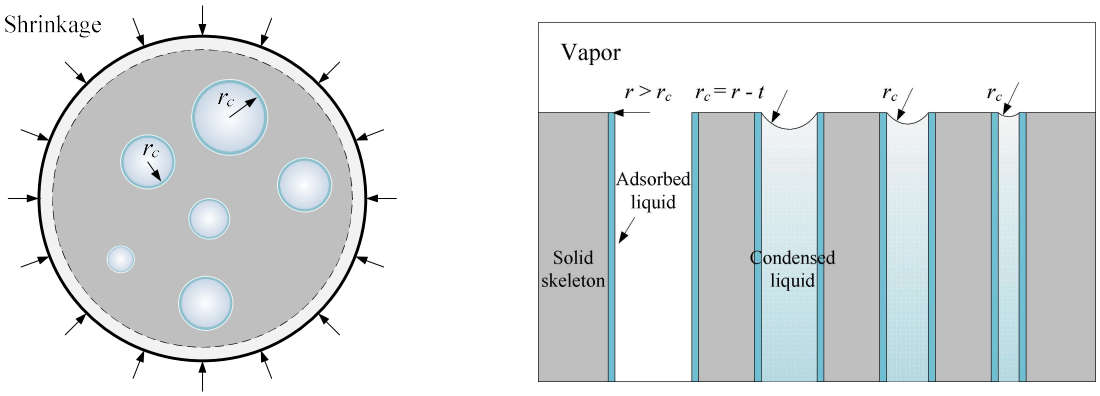

Fig. 3 Schematic illustration of the generation of capillary tension considering the effect of pore sizes, after [32].

Assuming that the whole paste at this stage are ideally elastic and isotropic, the autogenous shrinkage ε_c resulting from the induced capillary tension therefore can be expressed as [32]

$$\varepsilon_c = -\frac{1}{3}\left(\frac{1}{K_b} - \frac{1}{K_s}\right)\int_0^{r_{\max}} \left[P_c(r)\cdot f(r)\right] \mathrm{d}r \tag{3}$$

where K_b and K_s are the bulk moduli of the whole porous body and solid skeleton, respectively; $P_c(r)$ is the capillary tension in the pores with a radius of r; $f(r)$ is the probability density function of the volume of pores with a radius of r. Considering the fact that the capillary tension is only generated in the pore whose radius is smaller than the radius of menisci that corresponds to the give relative humidity *RH*, Eq. (3) can be rewritten as

$$\varepsilon_c = -\int_0^{r_c} f(r)\,\mathrm{d}r \cdot \frac{1}{3}\left(\frac{1}{K_b} - \frac{1}{K_s}\right) P_c \tag{4}$$

It is interesting to find that when the amount of adsorbed water is negligible in comparison with that of capillary water, the term of $\int_0^{r_c} f(r)$ physically approaches the degree of saturation S_w, which is defined as the ratio of the volume of saturated pores to the total pore volume. With this, the linear relationship between autogenous shrinkage ε_c and degree of saturation S_w is established [31,35,36],

$$\varepsilon_c = -\frac{S_w}{3}\left(\frac{1}{K_b} - \frac{1}{K_s}\right)P_c \tag{5}$$

3. Time-dependent autogenous shrinkage model

However, considering the fact that concrete, or, more accurately, the cement paste within the concrete, is a mixture of many kinds of compounds including C_3S, C_2S, and C_3A and ferrite-based phases, and each of them will react with water to form varying hydrates in different rates [37]. Thus, the physicochemical properties of cement paste have long been understood to evolve gradually as the cementation process advances.

As such, taking the effects of curing time into account, the autogenous shrinkage of HPC, $\varepsilon_c(t)$, during the cement hydration is defined as a variable which changes as a function of time t, accordingly, it is rewritten as:

$$\varepsilon_c(t) = -\frac{S_w(t)}{3}\left(\frac{1}{K_b(t)} - \frac{1}{K_s(t)}\right)P_c(t) \tag{6}$$

in which the time-dependent evolutions of capillary tension $P_c(t)$, degree of saturation $S_w(t)$, and porous body modulus $K_b(t)$ and solid skeleton modulus $K_s(t)$ all are regarded to be closely associated with the age of concrete.

In this section, based on the aforementioned capillary tension theory, a time-dependent model for determining the autogenous shrinkage of HPC is proposed, in which three respective prediction models for relative humidity, degree of hydration, and elastic modulus are adopted. The main methodology for the establishment of the model is briefly illustrated in Fig. 4.

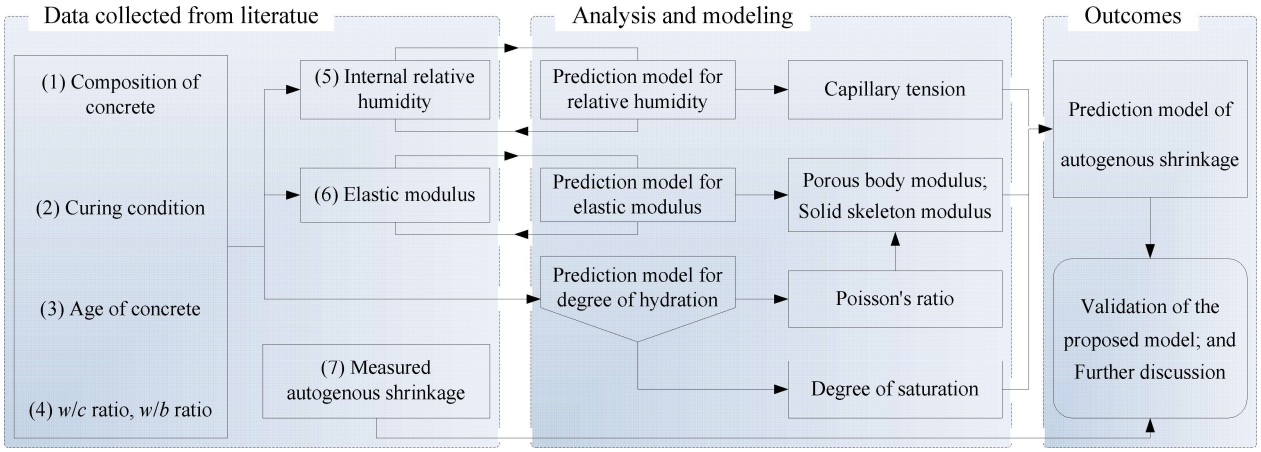

Fig. 4 Overview of the methodology for establishing the predictive model for real-time autogenous shrinkage.

3.1 Capillary tension $P_c(t)$

As stated earlier, autogenous shrinkage is the direct consequence of the decline of relative humidity due to self-desiccation over time. This phenomenon can be theoretically explained by the induced variation of capillary tension, $P_c(t)$, during the cementation process,

$$P_c(t) = -\frac{\rho RT \ln\left[RH(t)/100\right]}{M} \tag{7}$$

which acts as the main driving force in the formation of shrinkage. Hence, an exact determination of real-time relative humidity $RH(t)$ is of vital significance in predicting the capillary tension accurately.

To date, significant progress has been made on developing models that can predict the moisture transport within concrete [38]. In this study, for practical purpose, the empirical piecewise model suggested by [39] is adopted, in

which the two most crucial factors, i.e., w/c ratio and curing age, are taken into consideration,

$$RH(t)=\begin{cases}100 & t\le T_{cri}\\ 100+a_t\sqrt{w/c}+b_t & T_{cri}\le t\le 28\,\mathrm{d}\end{cases} \tag{8}$$

where t is the age of concrete (1 d $\le t \le$ 28 d, in unit of day); a_t and b_t are parameters related to the age of concrete, defined as $a_t = 7.295 + 20.586\ln(t)$, $b_t = -1.822 - 17.052\ln(t)$, respectively; T_{cri} is the critical time (in unit of day), given as $T_{cri} = \alpha \times (w/c)^2 + \beta \times (w/c) + \gamma$, in which α, β, and γ are the parameters determined with regression analysis of experimental data, and in general, $\alpha = 31.092$, $\beta = -16.983$, and $\gamma = 3.218$ are recommended under normal circumstances.

3.2 Degree of saturation $S_w(t)$

It is well known that in fresh concrete, almost all pores are initially filled with water, which however will gradually change into an unsaturated state due to the continuous water consumption in the hydration process. Hence, strictly speaking, concrete should be treated as a partially saturated porous construction material composed of vast aggregates, cement pastes and water in various forms, as shown in Fig. 5.

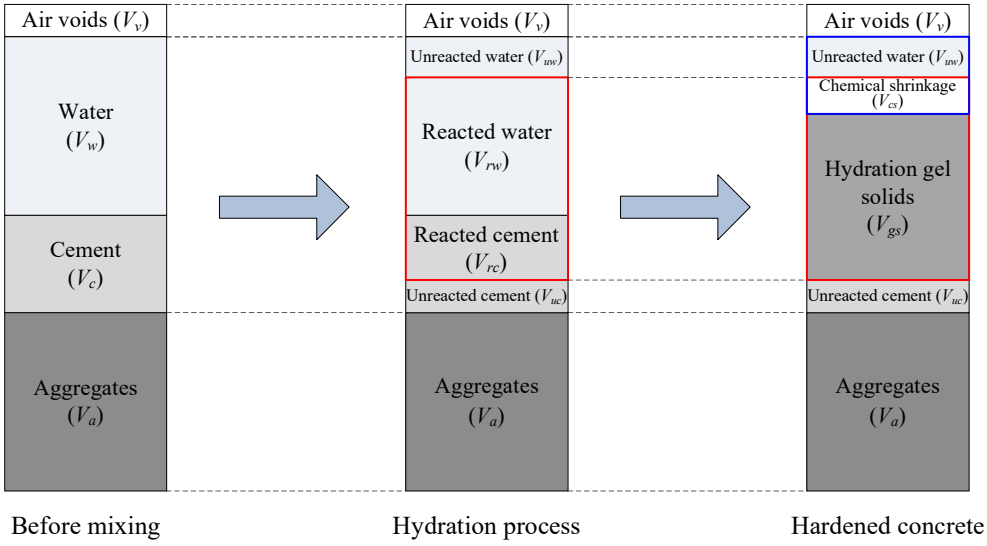

Fig. 5 Evolution of the volume of various components during the cementation process.

According to the Powers' volumetric model [40], during the hydration process, the water retained in cement pastes can be generally classified into three phases, namely, capillary water (free water), gel water (physically bound water), and non-evaporable water (chemically bound water). Among them, the former two phases are highly related to the degree of saturation, which are empirically given as,

$$V_{cw} = p - 1.32(1-p)\alpha \tag{9}$$

$$V_{gw} = 0.6(1-p)\alpha \tag{10}$$

where V_{cw} and V_{gw} are the volumes of capillary water and gel water, respectively; α is the degree of hydration (kg cement reacted/kg initial cement); p is the initial porosity, defined as $p = (w/c)/(w/c + \rho_w/\rho_c)$, in which ρ_w and ρ_c are the densities of water and cement, respectively. Moreover, it is also found that the volume of the formed gel solids is always smaller than the superposition of cement and water reacted, and this volume reduction, termed chemical shrinkage V_{cs}, approximately amounts to 6.4 ml/100 g cement reacted, i.e.,

$$V_{cs} = 6.4\times10^{-5}\rho_c(1-p)\alpha = 0.2(1-p)\alpha \tag{11}$$

Hence, the degree of saturation S_w is expressed as

$$S_w = \frac{V_{cw} + V_{cw}}{V_{cw} + V_{cw} + V_{cs}} = \frac{p - 0.72(1-p)\alpha}{p - 0.52(1-p)\alpha} \tag{12}$$

Given the evolution of hydration, the following equation is suggested to describe the time-development of saturation degree:

$$S_w(t) = \frac{p - 0.72(1-p)\alpha(t)}{p - 0.52(1-p)\alpha(t)} \tag{13}$$

where the degree of hydration $\alpha(t)$ here is a time-dependent variable that can be determined by the recommended equation in previous works [41],

$$\alpha(t) = 0.72\left(\frac{t}{30}\right)^{0.09} \exp\left[-\frac{0.01(t/30)^{0.07}}{w/b}\right] \tag{14}$$

where w/b is the water to binder ratio.

In the case of incorporation of silica fume to enhance the strength of HPC, the degree of saturation should be further refined as [42],

$$S_w(t) = \frac{p - 0.72k(1-p)\alpha(t)}{p - k\left[0.52 - 0.69(s/c)\right](1-p)\alpha(t)} \tag{15}$$

where the initial porosity $p = (w/c)/[w/c + \rho_w/\rho_c + (\rho_w/\rho_s)(s/c)]$, and s and c are the weight of silica fume and cement, respectively; $k = 1/[1 + (\rho_c/\rho_s)(s/c)]$, and ρ_s is the density of silica fume.

3.3 Porous body modulus $K_b(t)$ and solid skeleton modulus $K_s(t)$

As illustrated in Fig. 5, with the cement hydration advances, the induced volume reduction cannot be completely reflected by the macroscopic measured shrinkage, due to the gradual formation of the solid skeleton. The volumetric unbalance is compensated by the larger number of capillary pores formed within the pastes.

For such a porous cementitious material, the bulk modulus of the whole paste K_b is commonly calculated using the following formula [43],

$$K_b = \frac{E}{3(1-2\upsilon)} \tag{16}$$

where E is the elastic modulus, and υ is the Poisson's ratio. However, instead of assuming a constant value of 0.2 for Poisson's ratio, the bulk modulus of the whole paste in this study is modeled as a continuous development against the degree of hydration which relates to the age of concrete [44], as follows,

$$K_b(t) = \frac{E(t)}{3\left[1 - 2\upsilon(\alpha)\right]} \tag{17}$$

and

$$\upsilon(\alpha) = 0.18\sin\left[\frac{\pi\alpha(t)}{2}\right] + 0.5\exp\left[-10\alpha(t)\right] \tag{18}$$

For the bulk modulus of the solid skeleton $K_s(t)$, it can be further obtained in terms of the bulk modulus of the whole paste $K_b(t)$, the shear modulus $G_s(t)$, and its initial porosity p, upon the poromechanical approach [45],

$$K_s(t) = \frac{4G_s(t)K_b(t)}{4G_s(t)(1-p) - 3pK_b(t)} \tag{19}$$

For simplification, a constant value of $G_s(t)$ = 19.1 GPa is adopted. Hence, from Eqs. (17) and (19), it can be seen that the generation of the bulk moduli of both the whole porous body and skeleton solids is largely dependent on

the knowledge of elastic modulus evolution, which considerably determines the magnitude of the autogenous shrinkage.

Extensive experimental results have demonstrated that the evolution of elastic modulus is characterized by the feature that it increases rapidly at an early age of 1-7 d, while the growth rate tends to level off after 28 d [46], as shown in Fig. 6 (a). Hence, a non-linear exponential model was proposed as the form,

$$E(t) = E_{28}\left[1-\exp(-At)\right] \tag{20}$$

where E_{28} is the 28 d elastic modulus, and A is a constant that can be determined by experimental results. Through the regression analysis of several existing research, as shown in Fig. 6 (b), the calculation of E_{28} considering the variations of w/c is given,

$$E_{28} = 93.58\exp\left[-3.2(w/c)\right] \tag{21}$$

With all preceding definitions in mind, it becomes evident that by introducing Eqs. (7), (15), (17), and (19)) into Eq. (6), the real-time shrinkage $\varepsilon_c(t)$ is expected to be obtained with only a few parameter inputs, such as water to cement (binder) ratio, curing age, mix compositions, etc.

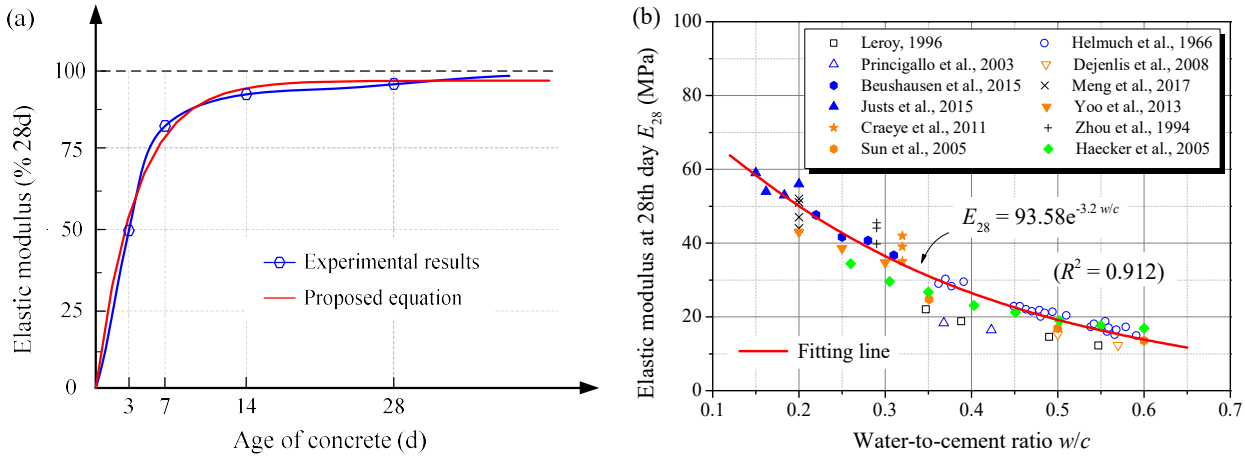

Fig. 6 Evolution of elastic modulus at early age and the determination of E_{28}.

4. Model validation

In this section, to validate the applicability of the proposed time-dependent model, four typical experimental research particularly targeting the autogenous shrinkage of HPC were chosen firstly, involving different kinds of concrete types. Secondly, upon an individual experiment study, the analytical predictions of the proposed model were compared with several commonly used formulas for further validation.

4.1 Comparisons between individual experimental results

For the selection of experimental cases, the main strategy was to ensure both the data of internal relative humidity against curing age and corresponding autogenous shrinkage are available, making the comparisons more reliable. Moreover, to isolate the interferences from other types of shrinkage as much as possible, the test specimens should be cured in a sealed condition and the water-to-binder ratio should be around or smaller than 0.4.

With these intentions, the following four experimental cases were adopted for comparison:

Case I: To investigate the effects of water-binder ratio and coarse aggregate on internal humidity and shrinkage of concrete, Zhang et al. [47] conducted a series of tests, of which three groups of high strength concrete (≈ 80 MPa) were sealed curing for autogenous shrinkage measurement. During the whole test, the relative humidity at the center of the specimen and its longitudinal deformation were measured simultaneously using a two-in-one setup, as

shown in Fig. 7 (a).

Case II: A little earlier, Li et al. [48] also conducted a similar experimental study, of which both the fine and coarse aggregates, however, were excluded. The relative humidity of the hardened cement paste was continuously recorded through a single setup (Fig. 7 (b)), while the autogenous shrinkage was measured using another prismatic specimen from the same batch.

Case III: In 2010, Hu et al. [49] performed some tests on the autogenous shrinkage of cement-based specimens mixed with fly ash, a type of supplementary cementitious material. The influences of expansive agent and different water-releasing materials on the variations of internal relative humidity and autogenous shrinkage were emphatically analyzed.

Case IV: To control the internal relative humidity and reduce early autogenous shrinkage, Ye et al. [50] replaced some proportions of coarse aggregate with pre-wetted light-weight aggregate. Based on the test results, the relationship between the content of water carrying and the autogenous shrinkage at 28 d was discussed.

The detailed information about the above four cases was summarized in Table 1. It should be noted that for simplification, only one group of the specimens was finally compared for each case.

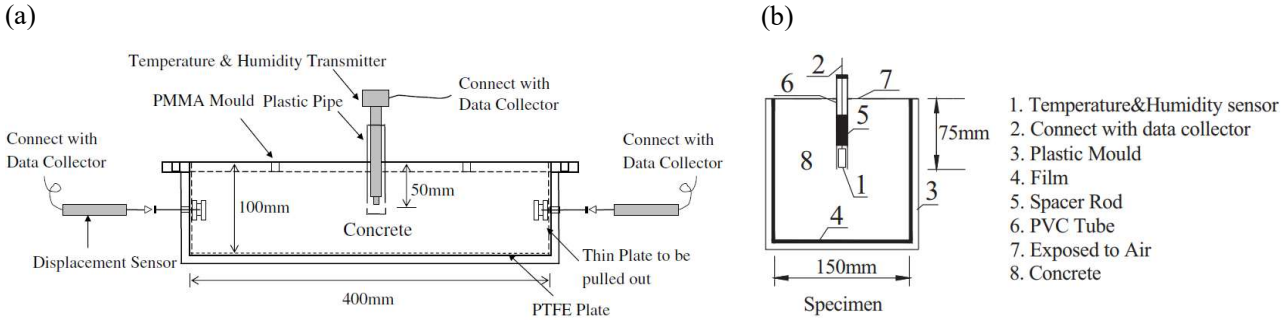

Fig. 7 Typical schematic diagram of the setup for internal relative humidity and shrinkage measurement, (a) two-in-one setup [47]; (b) single *IRH* measurement setup [46].

Table 1

Detailed information obtained from the literature.

Items	Data collected from references			
	Zhang et al., 2014 [47]	Li et al., 2013 [48]	Hu et al., 2010 [49]	Ye et al., 2006 [50]
Sample ID	C80-V60	A-1	2#	No.5
Specimen size (mm)	60 × 100 × 400	50 × 50 × 50 [a]	150 × 150 × 150 [a]	150 × 150 × 150 [a]
		40 × 40 × 160 [b]	100 × 100 × 515 [b]	100 × 100 × 300 [b]
Cement content (kg/m^3)	552.6	1800	450	423.5
Fly ash content (kg/m^3)	-	-	50	105.9
Silica fume content (kg/m^3)	61.4	-	-	-
Coarse aggregate (kg/m^3)	894.3	-	900	852.1
Fine aggregate (kg/m^3)	712.3	-	640	319.5
Water content (kg/m^3)	184.2	540	145	180.0
Curing temperature (°C)	23 ± 2	20 ± 2	20 ± 2	20 ± 3
w/*c* ratio	0.33	0.30	0.32	0.42
w/*b* ratio	0.30	0.30	0.29	0.34

SF percentage (%)	10	-	-	-
Initial porosity	0.479	0.486	0.477	0.517
Curing age (d)	28	56[a] / 28[b]	90	28

Note: [a] refers to the samples for relative humidity measurement, and [b] refers to the samples for autogenous shrinkage measurement.

The comparisons between the measured autogenous shrinkage, as well as internal relative humidity, from different experimental cases and the predicted values obtained from the proposed time-dependent model are shown in Fig. 8. It is clear that although some discrepancies are observed at the beginning of cement hydration, the analytical predictions agree quite well with the test results in general, and the main feature that autogenous shrinkage has an initial high rate and then gradually slows down with age was captured.

With respect to the underestimation of the measured results commonly observed in Fig. 8, it can be mainly attributed to the fact that the proposed model is purely developed based on the capillary tension approach, which assumes an elastic behavior of cementitious paste. Theoretically, this approach is only valid for a fully saturated linear elastic material, and at partial saturation state, it is approximate. Moreover, given the contributions of creep and plastic deformation of the hardening paste are not taken into consideration, the model therefore can only account for part of the measured shrinkage.

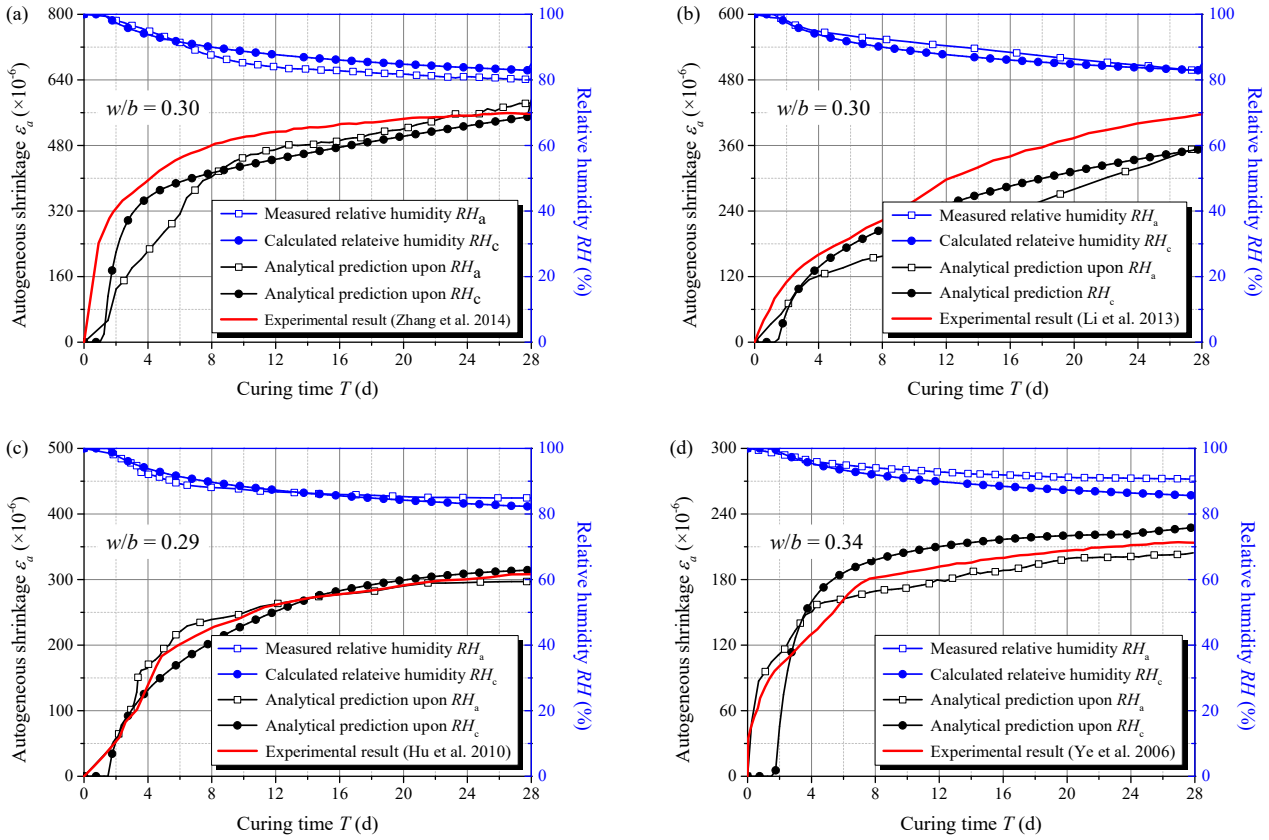

Fig. 8 Comparison between the test results from different references and analytical predictions obtained from the proposed model.

4.2 Comparisons between typical prediction formulas

For the purpose to compare the proposed model to other commonly used formulas, the experimental research conducted by Mazloom et al. [51] was quoted for further validation. In their study, to overcome the shortfall that the development of high strength concrete is generally at the cost of low workability, the component of cement was

partially replaced by silica fume. Four cylinder specimens of 80 mm × 270 mm (diameter × height) with different percentages of silica fume (0, 6%, 10%, and 15%) were cured in water for 7 days, followed by a sealed curing in a controlled environment of 20 ± 2 ℃ and 50 ± 5 % *RH* throughout the whole test duration. The details related to these four specimens are summarized in Table 2.

Table 2

Detailed information obtained from the Mazloom et al [51].

Items	Concrete mixes			
	OPC	SF6	SF10	SF15
Cement content (kg/m^3)	500	470	450	425
Silica fume content (kg/m^3)	-	30	50	75
Aggregate content (kg/m^3)	1850	1850	1850	1850
Water content (kg/m^3)	184.2	540	145	180.0
w/*c* ratio	0.35	0.37	0.39	0.41
w/*b* ratio	0.35	0.35	0.35	0.35
SF content (%)	0	6	10	15
Initial porosity	0.524	0.519	0.516	0.510
28 d compressive strength (MPa)	58	65	67.5	70

To estimate the autogenous shrinkage of high-strength concrete with silica fume more accurately, an alternative empirical prediction model based on the test results was suggested by them,

$$\varepsilon_c(t)_{\mathrm{MRB}} = 516t\frac{1.4\mathrm{SF}+0.39}{30\mathrm{SF}+12.6+t}\times 10^{-6} \tag{22}$$

where SF is the mass percentage of silica fume, i.e. SF = s / (s + c). It is worth noting that the period of shrinkage monitoring was not only limited to an early age but a long time of 587 d, due to the concern of the long-term property.

Three typical formulas in different codes specified for the estimation of shrinkage as follow were also referenced,

1. *ACI 209* [24]:

$$\varepsilon_c(t)_{\mathrm{ACI\text{-}209}} = 780\times 10^{-6}\frac{t}{35+t}\times\begin{cases}(1.4-0.01RH) & 40\le RH\le 80\\ (3.0-0.03RH) & 80< RH\le 100\end{cases} \tag{23}$$

2. *Eurocode 2* [25]:

$$\varepsilon_c(t)_{\mathrm{EN\text{-}2}} = 2.5(f_{ck}-10)\left[1-\exp\left(-0.2\sqrt{t}\right)\right]\times 10^{-6} \tag{24}$$

where f_{ck} is the characteristic compressive strength of concrete at the age of 28 d.

3. *Model Code 2010* [26]:

$$\varepsilon_c(t)_{\mathrm{MC\text{-}2010}} = \alpha_{as}\left(\frac{f_{cm}/10}{6+f_{cm}/10}\right)^{2.5}\left[1-\exp\left(-0.2\sqrt{t}\right)\right]\times 10^{-6} \tag{25}$$

where f_{cm} is the mean compressive strength of concrete at the age of 28 d, defined as f_{cm} = f_{ck} + 8 MPa; α_{as} is a coefficient related to the cement type, and the values of 800, 700, and 600 are recommended for a cement of types 32.5 N, 32.5 R/42.5 N, and 42.5 R/52.5N/52.5 R, respectively.

Having the above formulas, the development of predicted autogenous shrinkage against time, as well as measured real-time values, are plotted in Fig. 9. From the comparisons, the following observations can be seen,

i) Among all of the formulas, the proposed time-dependent model exhibits the best accuracy in the whole measuring period, even though it is originally aimed at the prediction of early age property. The influence of silica fume that the autogenous shrinkage of concrete increases as its amount increases is reasonably reflected. This implies that the proposed model is of great potential ability to estimate the long-term autogenous shrinkage of HPC containing different amounts of silica fume.

ii) The fitting model suggested by Mazloom et al. also shows a good agreement in spite of an obvious overestimation of the shrinkage in the early stage of the test. Owing to the satisfactory agreement with the measured autogenous shrinkage in the late stage, this empirical model therefore is particularly suitable for the evaluation of the long-term deformation.

iii) The formula from ACI 209 significantly overestimates the development of autogenous shrinkage, while the formula from Eurocode 2 shows a great underestimation, especially in the late stage. The main reason for the former is that basically, it is more suitable for calculating the collective contributions of all types of shrinkage, including autogenous shrinkage, drying shrinkage, carbonation shrinkage, etc. The latter is probably due to the inappropriate application range of formula, which seems to be more adequate for the early age prediction.

iv) The formula from Model Code 2010 exhibits an acceptable accuracy in the case of silica fume-free, which however becomes more conservative as the amount of silica fume increases, albeit a slight increase of shrinkage is observed. This suggests that the contribution of silica fume in facilitating the development of autogenous shrinkage is not well represented in this model.

Hence, to sum up, from the viewpoint of application, the models suggested by Eurocode 2 and Mazloom et al. are more suitable for predicting the short- and long-term deformations, respectively; the formula of Model Code 2010 is more adequate for the estimation of HPC without silica fume; while the proposed model in this study, based on a sound theoretical background, represents a compromise between accuracy and generality.

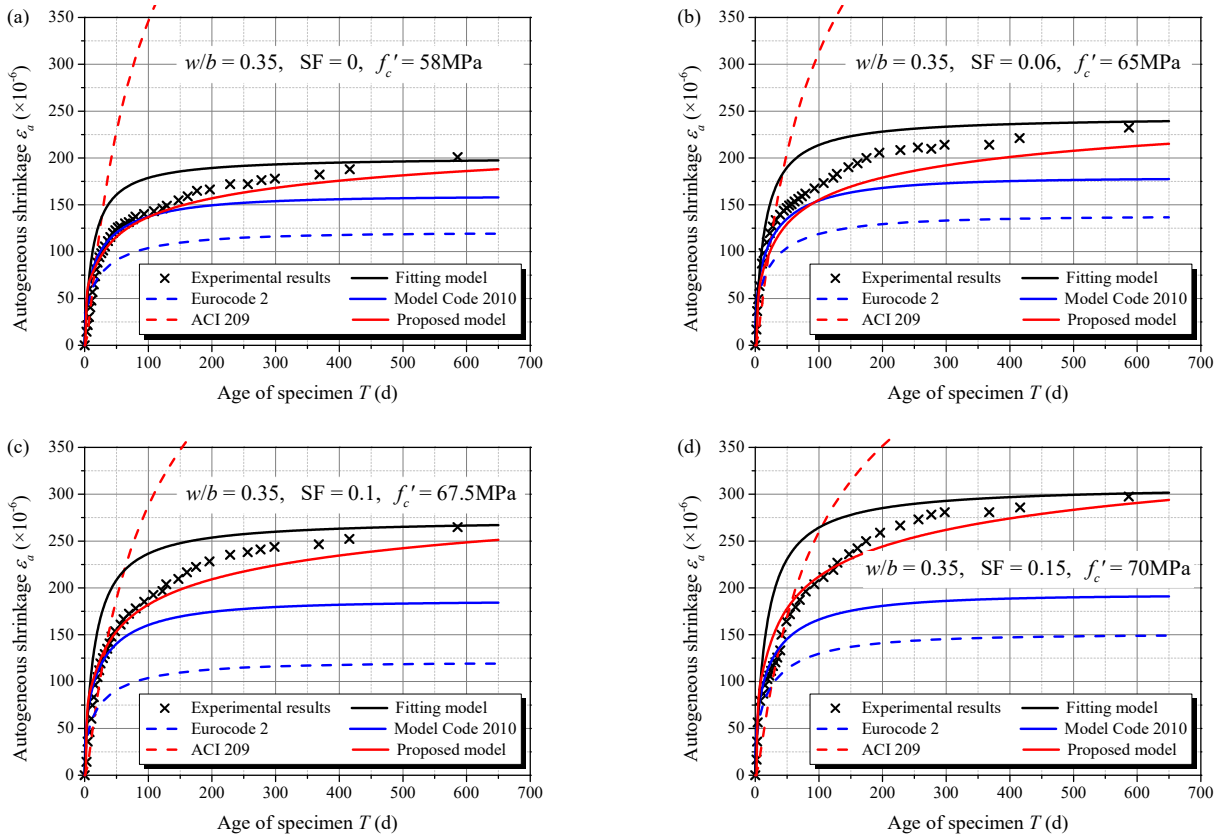

Fig. 9 Comparison between the test results and analytical predictions obtained from different formulas, considering the effect of silica fume on the evolution of autogenous shrinkage.

5. Conclusions

In this study, based on the capillary tension theory, a time-dependent model for evaluating the autogenous shrinkage of high performance concrete was proposed. To this end, hundreds of data points from tens of literature in terms of the composition of concrete, curing condition, age of concrete, water-to-cement (binder) ratio, internal relative humidity, elastic modulus, and measured autogenous shrinkage were selectively collected. Through a number of comparisons between analytical predictions and independent experimental results, the following conclusions can be drawn:

(1) Upon appropriate evolution laws of capillary tension, degree of saturation, porous body modulus and solid skeleton modulus, the time-dependent autogenous shrinkage of HPC can be reasonably predicted by means of the capillary tension approach.

(2) Taking the change of saturation degree during the hydration process into consideration, the effect of silica fume on the development of autogenous shrinkage can be well reflected within the proposed model.

(3) Due to the inherent shortfall of the capillary tension approach that assumes an elastic behavior of cementitious paste, plus the neglect of the contributions of creep and plastic deformation, the proposed model is prone to slightly underestimate the development of autogenous shrinkage.

(4) Compared with the commonly used formulas in different codes, the proposed model exhibits a consistent agreement with the measured value in a long-time range in general, representing a compromise between accuracy and generality of application.

Acknowledgements

The work presented herein was funded by the University of Hong Kong through Seed Grant for Basic Research. The financial support is gratefully acknowledged.

References

[1] Aïtcin PC. High performance concrete. CRC press, 2011.

[2] Pimienta P, Robert JM, Jean-Christophe M. Physical properties and behaviour of high-performance concrete at high temperature: State-of-the-Art Report of the RILEM Technical Committee 227-HPB. Vol. 29. Springer, 2018.

[3] Wyrzykowski M, Terrasi G, Lura P. Expansive high-performance concrete for chemical-prestress applications. Cement Concrete Res, 2018, 107: 275-283.

[4] Arora A, Aguayo M, Hansen H, Castro C, Federspiel E, Mobasher B, Neithalath N. Microstructural packing-and rheology-based binder selection and characterization for ultra-high performance concrete (UHPC). Cement Concrete Res, 2018, 103: 179-190.

[5] Shi Y, Long G, Ma C, Xie Y, He J. Design and preparation of ultra-high performance concrete with low environmental impact. J Clean Prod, 2019, 214: 633-643.

[6] Hafiz M A, Hajiesmaeili A, Denarié E. Tensile response of low clinker UHPFRC subjected to fully restrained shrinkage. Cement Concrete Res, 2019, 124: 105804.

[7] He Z, Du S, Chen D. Microstructure of ultra high performance concrete containing lithium slag. J Hazard Mater, 2018, 353: 35-43.

[8] Zhou M, Lu W, Song J, Lee GC. Application of ultra-high performance concrete in bridge engineering. Constr Build Mater, 2018, 186: 1256-1267.

[9] Rasoolinejad M, Rahimi-Aghdam S, Bažant Z P. Prediction of autogenous shrinkage in concrete from material

composition or strength calibrated by a large database, as update to model B4. Mater Struct, 2019, 52(2): 33.
[10] Wu L, Farzadnia N, Shi C, Zhang Z, Wang H. Autogenous shrinkage of high performance concrete: A review. Constr Build Mater, 2017, 149: 62-75.
[11] Ghafari E, Ghahari SA, Costa H, Júlio E, Portugal A, Durães L. Effect of supplementary cementitious materials on autogenous shrinkage of ultra-high performance concrete. Constr Build Mater, 2016, 127: 43-48.
[12] Sant G. The influence of temperature on autogenous volume changes in cementitious materials containing shrinkage reducing admixtures. Cement Concrete Comp, 2012, 34(7): 855-865.
[13] Kumarappa DB, Peethamparan S, Ngami M. Autogenous shrinkage of alkali activated slag mortars: Basic mechanisms and mitigation methods. Cement Concrete Res, 2018, 109: 1-9.
[14] Lee K M, Lee H K, Lee S H, Kim GY. Autogenous shrinkage of concrete containing granulated blast-furnace slag. Cement Concrete Res, 2006, 36(7): 1279-1285.
[15] Ye H, Radlińska A. Shrinkage mitigation strategies in alkali-activated slag. Cement Concrete Res, 2017, 101: 131-143.
[16] Ye H, Cartwright C, Rajabipour F, Radlińska A. Understanding the drying shrinkage performance of alkali-activated slag mortars. Cement Concrete Comp, 2017, 76: 13-24.
[17] Kang SH, Hong SG, Moon J. Importance of drying to control internal curing effects on field casting ultra-high performance concrete. Cement Concrete Res, 2018, 108: 20-30.
[18] Chylík R, Fládr J, Bílý P, Trtík T, Vráblík L. An analysis of the applicability of existing shrinkage prediction models to concretes containing steel fibres or crumb rubber. Journal of Building Engineering, 2019, 24: 100729.
[19] Li Y, Li J. Capillary tension theory for prediction of early autogenous shrinkage of self-consolidating concrete. Constr Build Mater, 2014, 53: 511-516.
[20] Ghourchian S, Wyrzykowski M, Lura P. A poromechanics model for plastic shrinkage of fresh cementitious materials. Cement Concrete Res, 2018, 109: 120-132.
[21] Carette J, Staquet S. Unified modelling of the temperature effect on the autogenous deformations of cement-based materials. Cement Concrete Comp, 2018, 94: 62-71.
[22] Nehdi ML, Soliman AM. Artificial intelligence model for early-age autogenous shrinkage of concrete. ACI Mater J, 2012, 109(3).
[23] Japan Society of Civil Engineers (JSCE). Standard specification for concrete structures. Structural performance verification, 2007.
[24] ACI Committee 209. Prediction of creep, shrinkage and temperature effects in concrete structures. ACI Manual of concrete practice, Part 1, 1997, 209R 1-92.
[25] Comite´ Europe´en de Normalisation. Design of concrete structures, part 1-1: general rules and rules for buildings. Eurocode 2, EN 1992-1-1, 2004.
[26] Model Code 2010. International Federation for Structural concrete (fib), Final draft, Lausanne, Switzerland, 2011.
[27] Jennings HM. Refinements to colloid model of CSH in cement: CM-II. Cement Concrete Res, 2008, 38(3): 275-289.
[28] Rezvani M, Proske T, Graubner CA. Modelling the drying shrinkage of concrete made with limestone-rich cements. Cement Concrete Res, 2019, 115: 160-175.
[29] Gardner NJ, Lockman MJ. Design provisions for drying shrinkage and creep of normal-strength concrete. ACI Mater J, 2001, 98(2): 159-167.
[30] López V, Pacios A. Modelling the influence of SRA on properties of hpc. Measuring, Monitoring and Modeling Concrete Properties. Springer, Dordrecht, 2006.
[31] Lura P, Jensen OM, Van Breugel K. Autogenous shrinkage in high-performance cement paste: An evaluation of basic mechanisms. Cement Concrete Res, 2003, 33(2): 223-232.
[32] Ye H, Radlińska A. A review and comparative study of existing shrinkage prediction models for portland and non-portland cementitious materials. Adv Mater Sci Eng, 2016, 2016.
[33] Butt HJ, Graf K, Kappl M. Physics and chemistry of interfaces. John Wiley & Sons, 2013.
[34] Wei Y, Xiang Y, Zhang Q. Internal curing efficiency of prewetted LWFAs on concrete humidity and

autogenous shrinkage development. J Mater Civil Eng, 2013, 26(5): 947-954.
[35] Bentz DP, Jensen OM. Mitigation strategies for autogenous shrinkage cracking. Cement Concrete Comp, 2004, 26(6): 677-685.
[36] Lura P. Autogenous deformation and internal curing of concrete. 2003.
[37] Pang X, Meyer C. Cement chemical shrinkage as measure of hydration kinetics and its relationship with nonevaporable water. ACI Mater J, 2012, 109(3): 341.
[38] Zhang J, Qi K, Huang Y. Calculation of moisture distribution in early-age concrete. J Eng Mech, 2009, 135(8): 871-880.
[39] Shen D, Wang M, Chen Y, Wang T, Zhang J. Prediction model for relative humidity of early-age internally cured concrete with pre-wetted lightweight aggregates. Constr Build Mater, 2017, 144: 717-727.
[40] Jensen OM, Hansen PF. Water-entrained cement-based materials: I. Principles and theoretical background. Cement Concrete Res, 2001, 31(4): 647-654.
[41] Ye H, Jin X, Chen W, Fu C, Jin N. Prediction of chloride binding isotherms for blended cements. Comput Concr, 2016, 17(5): 655-672.
[42] Zhang J, Hou D, Gao Y. Calculation of shrinkage stress in early-age concrete pavements. I: Calculation of shrinkage strain. J Transp Eng, 2012, 139(10): 961-970.
[43] Aili A, Vandamme M, Torrenti JM, Masson B. Is long-term autogenous shrinkage a creep phenomenon induced by capillary effects due to self-desiccation?. Cement Concrete Res, 2018, 108: 186-200.
[44] De Schutter G, Taerwe L. Degree of hydration-based description of mechanical properties of early age concrete. Mater Struct, 1996, 29(6): 335.
[45] Zeng Q, Fen-Chong T, Dangla P, Li K. A study of freezing behavior of cementitious materials by poromechanical approach. Int J Solids and Struct, 2011, 48(22-23): 3267-3273.
[46] Shen D, Shi X, Zhu S, Duan X, Zhang J. Relationship between tensile Young's modulus and strength of fly ash high strength concrete at early age. Constr Build Mater, 2016, 123: 317-326.
[47] Zhang J, Han Y D, Gao Y. Effects of water-binder ratio and coarse aggregate content on interior humidity, autogenous shrinkage, and drying shrinkage of concrete. J Mater Civil Eng, 2013, 26(1): 184-189.
[48] Li Y, Yan QQ. Relationship between Internal Relative Humidity and Autogenous Shrinkage of Cement Paste with Supplementary Cementitious Materials (SCM). Key Engineering Materials, 2013, 539: 35-39.
[49] Hu S, Wu J, Yang W, et al. Relationship between autogenous deformation and internal relative humidity of high-strength expansive concrete. J Wuhan Univ Techno, 2010, 25(3): 504-508.
[50] Ye JJ, Hu SG, Wang FZ, Zhou YF, Liu ZC. Effect of pre-wetted light-weight aggregate on internal relative humidity and autogenous shrinkage of concrete. J Wuhan Univ Techno, 2006, 21(1): 134-137.
[51] Mazloom M, Ramezanianpour AA, Brooks JJ. Effect of silica fume on mechanical properties of high-strength concrete. Cement Concrete Comp, 2004, 26(4): 347-357.